Journal of Nuclear Materials 510 (2018) 585–595

Contents lists available at ScienceDirect

Journal of Nuclear Materials

journal homepage: www.elsevier.com/locate/jnucmat

Model of nuclear fuel pellets densification under irradiation and isothermal conditions: Application to UO_2 fuels

Mauricio E. Cazado [a, b, *], Alicia C. Denis [a, b]

[a] Sección Códigos y Modelos, Gerencia Ciclo del Combustible Nuclear, CNEA, Avenida General Paz 1499, 1650 San Martín, Buenos Aires, Argentina
[b] Instituto Sabato, UNSAM-CNEA, Avenida General Paz 1499, 1650 San Martín, Buenos Aires, Argentina

HIGHLIGHTS

- Modeling of fuel pellets densification under irradiation and thermal conditions.
- Simulation of point defects diffusion and interaction of fission spikes with pores.
- An acceptable and more realistic agreement with experimental data is obtained.

ARTICLE INFO

Article history:
Received 4 June 2018
Received in revised form
10 August 2018
Accepted 16 August 2018
Available online 17 August 2018

Keywords:
Nuclear fuel
Densification
Pores distribution
Crystal defects

ABSTRACT

The dimensional changes of a nuclear fuel in operation are strongly determined by two opposite effects. One of them is due to contraction of the as-fabricated pores, giving place to densification which is evident during the first stages of irradiation. This effect is counteracted by the swelling phenomenon provoked by the fission products that progressively accumulate in the fuel material. A model to evaluate the changes in fuel pellets porosity due to radiation and thermal effects taking into account the point defects flow to and from the pores is presented. A simplification of the model to assess the progress of porosity in isothermal re-sintering tests is also given. Simulations are compared with experimental data measured on UO_2 fuel pellets with a variety of microstructures at different temperatures and radiation conditions, attaining a good agreement.

1. Introduction

During fabrication of the nuclear fuel pellets, the uranium dioxide powder is sintered at high temperatures, resulting in a material with a density of 90–96% of the theoretical density of UO_2. The remaining porosity is necessary for accommodating, at least in part, the fission gases that are generated during fuel irradiation. In service, under the combined effects of temperature and radiation, the fabrication pores tend to reduce their size and consequently, the fuel material increases its density. Moreover, the fission gases, almost insoluble in the oxide matrix, precipitate forming bubbles, that are the main cause of the material swelling. The effect of densification dominates at low burnup while that of swelling, at intermediate and high burnup. Diverse phenomena, two of which are densification and swelling, cause dimensional changes in nuclear fuel rods and impose restrictions on reactor operation [1–3]. It is hence of great importance to have reliable calculation tools to predict them.

Several models taking into account point defects production, either of thermal origin or produced by irradiation, and their migration to and from sinks and sources, have been proposed [2,4–9]. The present work intends to make a contribution in this regard. The work by Assmann et al. [2] takes into account vacancies migration from the pore surface towards the grain boundary but ignores the effect of interstitials in densification. The model developed by Dollins et al. [4,5] considers the time evolution of pores, uniform in size, without considering its initial distribution. Tarasov and Veshchunov [9] assume that densification is well represented by the intergranular pores evolution without contemplating the effect of those within the grains. Lindman [7] proposes an empirical expression to give an account of the fuel density variation by means of several parameters that are fitted to experimental data, without analyzing the microstructural

* Corresponding author. Instituto Sabato, UNSAM-CNEA, Avenida General Paz 1499, 1650 San Martín, Buenos Aires, Argentina.
E-mail addresses: cazado@cnea.gov.ar (M.E. Cazado), denis@cnea.gov.ar (A.C. Denis).

https://doi.org/10.1016/j.jnucmat.2018.08.029
0022-3115/

mechanisms involved. The model presented in this work, which is based in many respects on those proposed by Veshchunov et al. [8] and Bouguerra et al. [6], includes some new considerations about the densification mechanism like the influence of the mechanical properties of the fuel material on the calculation of the interstitial-dislocation bias factor, the limiting effect of the lattice vacancies saturation on vacancies emission from a pore, among others.

Microscopy observations reveal that fabrication pores of different sizes are present at the grain boundaries (intergranular pores) and within the grains (intragranular pores) [10,11]. Irradiation experiments, like those reported by Ross [12], show that pores with radii smaller than 0.15 μm are completely eliminated even at burnup levels as low as 400 MW d/tU while larger pores remain longer in the lattice. This indicates that the initial pore size has a significant effect on the shrinkage rate and hence a realistic model of densification must include the pore size distribution. A similar point of view was used in the model elaborated by Tarasov and Veshchunov [13].

A model based on diffusion of vacancies and interstitials in the fuel lattice, aimed at evaluating pellet densification under irradiation conditions, is presented in this work and compared with experimental data. Additionally, a simplified model describing isothermal conditions in the absence of irradiation is derived from the former one and is also compared with experiments.

2. The model assumptions

2.1. Initial porosity distribution

According to Tarasov et al. [9,13], the fabrication pores are characterized by a *concentration distribution function* $n_p(r,t)$ such that $n_p(r,t)dr$ measures the number of pores per unit volume with radii between r and $r + dr$. Similarly, the *porosity distribution function* $p(r,t)$ is such that $p(r,t)dr$ represents the volume fraction occupied by the pores with radii between r and $r + dr$. Both parameters are related by $p(r,t) = n_p(r,t)V_p(r)$, where V_p represents the pore volume. In the present model, the pores concentration will be assumed to depend only on the radius: $n_p(r)$. Within this assumption, the porosity change is due only to variations in the pores size.

Whichever is the experimental technique used, a detection limit exists for the pore size, i.e., there is a given minimum radius R_c below which a pore cannot be detected. For simplicity, the present model assumes that in the initial pore distribution no pores exist with radii smaller than R_c. Furthermore, when due to the shrinkage process, the pore radius reduces below a given threshold (R_t), the pore is assumed to vanish and the small corresponding void volume is located at the pellet periphery.

The following expression for the concentration distribution is assumed to hold [9]:

$$n_p(r) = \begin{cases} 0 & r < R_c \\ \dfrac{n_0}{R_0} e^{-r/R_0}, & r \geq R_c \end{cases} \tag{1}$$

since it yields a monomodal porosity distribution, where n_0 and R_0 are fitting parameters of the distribution.

Some fresh fuel pellets present a bimodal porosity distribution [3] and expression (1) cannot be applied. For these cases a superposition of two concentration distributions is proposed:

$$n_p(r) = \begin{cases} 0 & r < R_c \\ \dfrac{n_{01}}{R_{01}} e^{-r/R_{01}} + \dfrac{n_{02}}{R_{02}} e^{-r/R_{02}}, & r \geq R_c \end{cases} \tag{2}$$

where n_{01}, n_{02}, R_{01} and R_{02} are fitting parameters that depend on the experimental conditions.

The model used in the present work for simulating the pores distribution is based on the following considerations:

I. A fresh fuel pellet can contain intra- and intergranular pores.
II. Intragranular pores are considered spherical while intergranular pores are assumed to have a lenticular shape, formed by the intersection of two spherical caps of the same radius ρ, intersecting at a dihedral angle $\theta = 50^\circ$, that on the grain boundary plane gives the projected pore radius $r = \rho \sin\theta$ [14].
III. For both types of pores, the volume and surface area are respectively given by $V = \frac{4}{3}\pi r^3 f_V$ and $A = 4\pi r^2 f_A$ where

$$f_V = \begin{cases} 1 & \text{, for intragranular pores} \\ \dfrac{1}{\sin^3\theta}\left(1 - \dfrac{3}{2}cos\theta + \dfrac{1}{2}\cos^3\theta\right), & \text{for intergranular pores} \end{cases} \tag{3}$$

$$f_A = \begin{cases} 1 & \text{, for intragranular pores} \\ \dfrac{1}{\sin^2\theta}(1 - cos\theta), & \text{for intergranular pores} \end{cases} \tag{4}$$

IV. In order that a grain can contain a pore within it, the pore radius needs to be less than a given fraction of the grain radius (R_g). In this work, this fraction is assumed as the fifth part of the mean grain radius.
V. Intergranular pores can adopt values in the entire spectrum of possible radii.
VI. Different criteria can be chosen to characterize the pores distribution. The mean value and the median are usually defined in terms of the number of pores, i.e., they are based on how frequently each pore size is observed. Alternatively, moments of higher order were analyzed by Leschonski [15] in connection with particles statistics. In the present work the following criterion is adopted to describe the mean volume pore radius:

$$r_{mv} = \frac{\int_0^\infty r^4 n_p(r)dr}{\int_0^\infty r^3 n_p(r)dr} \tag{5}$$

The median volume pore radius, that represents the radius up to which the distribution accumulates half of the total porosity, is implicitly defined by:

$$\int_0^{r_{medv}} V_p(r) n_p(r)dr = \frac{1}{2}\int_0^\infty V_p(r) n_p(r)dr \tag{6}$$

It will be important to know the relationship between these parameters and R_0 to solve (1) or (2), since r_{mv} or r_{medv} are usually provided by the experimental measurements. Assuming a monomodal distribution of intragranular pores, if $R_c = 0$, integration of (5) and (6) led to:

$$r_{mv} = 4R_0 \tag{7}$$

$$2e^{-\psi}\left[1 + \psi + \frac{1}{2}\psi^2 + \frac{1}{6}\psi^2\right] - 1 = 0 \tag{8}$$

and if $R_c \neq 0$, we have:

$$r_{mv} = 4R_0 + \frac{R_c}{\left[6\Gamma^3 + 6\Gamma^2 + 3\Gamma + 1\right]} \tag{9}$$

$$2e^{-r}\left[1 + \Gamma + \frac{1}{2}\Gamma^2 + \frac{1}{6}\Gamma^2\right] - 2e^{-\psi}\left[1 + \psi + \frac{1}{2}\psi^2 + \frac{1}{6}\psi^2\right] - 1 = 0 \tag{10}$$

where $\psi = r_{medv}/R_0$ and $\Gamma = R_c/R_0$. Equations (8)–(10) are quite complicated and have to be solved numerically. For bimodal distributions, the relationships for r_{mv} and r_{medv} become even more complex. The problem is partially simplified if both modes are sufficiently separated, which can be interpreted as two pores populations with no mutual interference. In this case, the ratio $\psi = r_{medv}/R_0$ can be assumed to have the same value for both peaks, each one with its own value of r_{medv}. Then, the respective values of R_0 are obtained and equation (2) can be solved.

VII. The treatment of the experimental data becomes simpler if pores are grouped into classes defined by radii intervals. The following law is proposed to identify the pore classes according to Ozrin et al. [16]:

$$r_j = R_0 10^{j/10} \qquad j = 1, 2, \ldots, n \tag{11}$$

The following approaches are developed to calculate the pores concentration and porosity corresponding to class j:

$$N_p(r_j) = \int_{r_j+\Delta^-}^{r_j+\Delta^+} n_p(r).dr \tag{12}$$

$$P(r_j) = \int_{r_j+\Delta^-}^{r_j+\Delta^+} \eta_p(r) \cdot V_p(r)\, dr = 8\pi f_V R_0^3 n_0 e^{-x}\left(1 + x + \frac{1}{2}x^2 + \frac{1}{6}x^3\right)\Bigg|_{r_j+\Delta^-}^{r_j+\Delta^+} \tag{13}$$

where $x = r/R_0$, $\Delta^+ = \frac{r_{j+1}-r_j}{2}$, $\Delta^- = \frac{r_j-r_{j-1}}{2}$ and f_V is given by (3).

2.2. Densification model

The densification mssssodel presented in this work is based on the premises listed below and takes into account the combined effects of irradiation and temperature. Moreover, a simplified version of the model is also presented in section 2.2.2, which considers the sole effect of temperature.

2.2.1. Densification under irradiation

The model assumes the following phenomena:

I. Fission of a uranium atom gives place to new neutrons and two highly energetic fission fragments. A fission fragment loses its energy when colliding with the lattice atoms, thus triggering a damage cascade. The atomic displacements give origin to different types of defects, in particular vacancies and interstitials. These point defects have a considerable probability of recombination but about 10% of them can migrate through the lattice [1,4] and reach different sinks. On the other hand, the spikes along their path have a certain probability of passing sufficiently close to a pore and provoke the release of a number of vacancies [2,17,18].

II. Dislocations, grain boundaries and pore surfaces can emit vacancies and can also act as sinks of vacancies and interstitials due to the sole effect of temperature.

III. A pore shrinks due to capture of interstitials and release of vacancies and expands due to capture of vacancies.

According to Veshchunov et al. [8], the generation rate of point defects by irradiation is given by:

$$\dot{K} = Y_{vi}\Omega\dot{F} \tag{14}$$

where Y_{vi} is the number of point defects that can escape from a damage cascade, estimated between 1×10^4 and 5×10^5 [19,20]; $\Omega = 4.09 \times 10^{-29}$ (m^3) is the atomic volume of the unit cell in UO_2 and $\dot{F}$ is the volumetric fission rate. If the spike interacts with an intragranular pore, the ejected vacancies can be assumed to remain within the grain containing the pore. But if it interacts with a pore in a grain boundary, the released vacancies are assumed to be collected by both neighboring grains with equal probability. For each pore class, the rate of vacancies produced per pore-spike interaction is [4,6,18,21]:

$$NK^a = 2\pi(r^a + r_{int})^2 N_p^a \Omega\dot{F}\eta\lambda f_{sat} f_{vl}^a \tag{15}$$

$$NK^e = \pi(r^e + r_{int})^2 N_p^e \Omega\dot{F}\eta\lambda f_{sat} f_{vl}^e \tag{16}$$

where the superscripts a and e stand for intragranular and intergranular pores, respectively; r is the pore radius; r_{int} is the range of interaction with a fission fragment; N_p is the concentration of pores; η is a fitting constant representing the number of vacancies that can be ejected from a void in a single interaction; λ is the fission fragment track length; f_{sat} is the vacancies saturation function; f_{vl} represents the vacancies volume fraction within a pore. The last two parameters are proposed to obey [21]:

$$f_{sat} = \max[0; 1 - C_v/C_{vsat}] \tag{17}$$

$$f_{vl} = 1 - n_g^0 b_{vw}/V_p \tag{18}$$

where C_v is the vacancies concentration in the bulk and C_{vsat} its saturation value; n_g^0 is the initial number of gas moles within a pore, composed solely by the sintering gas used in the manufacturing process of the pellets at the time when the pores turned out to be closed, usually He or H_2, and b_{vw} is the van der Waals volume of that gas.

Dislocations, grain boundaries, pores, vacancies and interstitials are the lattice defects considered in the present model. For simplicity, point defects (vacancies and interstitials) are assumed to verify the stoichiometric relation, i.e., to consist of one uranium cation and two oxygen anions. When point defects reach the vicinity of a dislocation, they can be captured making the dislocation to climb. The dislocation sink strength is given by Ref. [22]:

$$S_{d(v,i)} = \frac{2\pi\rho_D z_{v,i}}{ln\left(r_{md}/r_{cd(v)}\right)} \qquad \left(m^{-2}\right) \tag{19}$$

$$r_{md} \approx \frac{1}{\sqrt{\pi \rho_D}} \quad (m) \tag{20}$$

$$\rho_D = \max\left[10^{12}; \exp\left(-2.07 \times 10^{-3}(T-273)+21.82\right)\right] \quad \left(m^{-2}\right) \tag{21}$$

where r_{md} is the mean distance between dislocations; $r_{cd(v)}$ is the radius of the spontaneous capture of vacancies by dislocations; ρ_D is the dislocation density; T is the absolute temperature; $z_{v,i}$ is the dislocation bias factor for vacancies and interstitials, respectively. Considering that the dislocation-interstitial elastic interaction is stronger than that for dislocation-vacancy, the bias factor for interstitials should be higher than that for vacancies [23]. According to Baranov et al. [24] a relationship between z_v and z_i can be estimated using:

$$\frac{z_i}{z_v} = \frac{\ln\left(r_{md}/r_{cd(v)}\right)}{\ln\left(r_{md}/r_{cd(i)}\right)} \tag{22}$$

$$r_{cd(v,i)} = r_a + L_{v,i}/2 \tag{23}$$

where $r_{cd(i)}$ is the radius of spontaneous capture of interstitials by dislocations; $r_a \sim 5b$ is the dislocation core radius; b is the Burgers vector; $L_{v,i} = \left|\frac{(1+\mu)G\Delta V_{v,i}b}{3(1-\mu)k_bT\pi}\right|$; $\Delta V_{v,i}$ is the relaxation volume caused by the presence of point defects in the lattice [24]; k_b is the Boltzmann constant; G and μ are the shear modulus and Poisson ratio of UO_2 [1,25]:

$$\mu = 1.32(1-0.26P_T) - 1 \tag{24}$$

$$G = \frac{E}{2(1+\mu)} \tag{25}$$

$$E = 2.334 \times 10^{11}(1-2.752P_T) \times \left(1-1.0915 \times 10^{-4}T\right) \tag{26}$$

where P_T is the fuel total porosity and E is the elastic modulus.

As stated by Olander [1], for a pore class j, the pore sink strength can be approximated with the expression:

$$S_{p_j}^{(a,e)} = 4\pi r_{p_j}^{(a,e)} N_{p_j}^{(a,e)} \tag{27}$$

To estimate the grain boundary sink strength, the expression suggested by Brailsford [23] is applied here:

$$S_{GB(v,i)} = \frac{3}{R_g}\left(S_{d(v,i)} + \sum_{k=1}^{n} S_{p_k} + \sum_{l=1}^{m} S_{p_l}\right)^{1/2} \tag{28}$$

where n and m are the number of intragranular and intergranular pore classes, respectively. Then, the total sink strength is:

$$S_{t(v,i)} = S_{d(v,i)} + \sum_{k=1}^{n} S_{p(v,i)_k} + \sum_{l=1}^{m} S_{p(v,i)_l} + S_{GB(v,i)} \tag{29}$$

where the subscripts d, p and GB stand for dislocations, pores and grain boundaries, respectively. If an interstitial and a vacancy are as close as a few lattice parameters, they can recombine and the rate of this process is given by Ref. [8]:

$$IV = \alpha D_i C_i C_v \tag{30}$$

where D_i is the interstitial diffusion coefficient; C_i is the interstitial concentration in the bulk; $\alpha = 4\pi r_{vi}/\Omega$ is the vacancy-interstitial recombination constant; r_{vi} is the distance at which a vacancy and an interstitial can recombine, which can be approximated by the lattice parameter a [8,26]. Then $\alpha \cong 4\pi a/\Omega$. yields for α the estimation 1.68×10^{20} (m^{-2}) which is in good agreement with the value 10^{20} (m^{-2}) recommended by Griesmeyer et al. [27].

An important aspect of the model is the determination of vacancies and interstitials concentrations. To do so, the mean-field approximation is taken into account in the diffusion equations. In what follows, the point defects concentration is given as the fraction of defect sites per uranium atom in the lattice. The balance equations for point defects are given by Refs. [6,13,22,28]:

$$\frac{\partial C_v}{\partial t} = \dot{K} + \sum_{k=1}^{n}\left(S_{pv_k}D_vC_v^{ps} + NK_k^{(a)}\right) + \sum_{l=1}^{m}\left(S_{pv_l}D_vC_v^{ps} + NK_l^{(e)}\right) + (S_{dv} + S_{BGv})D_vC_v^{eq} - S_{tv}D_vC_v - IV \tag{31}$$

$$\frac{\partial C_i}{\partial t} = \dot{K} - S_{ti}D_iC_i - IV \tag{32}$$

where C_v^{ps} is the vacancies concentration on the pore surface and D_v is the diffusion coefficient of vacancies in the bulk.

The diffusive processes in UO_2 involve the migration of both atomic species altogether; the rate determinant species (the slower one) is the uranium cation. The interstitial bulk diffusion coefficient is calculated with:

$$D_i = \left(\frac{a}{2}\right)^2 \upsilon_i \exp\left(-\frac{E_{im}}{RT}\right) \tag{33}$$

where $\upsilon_i = 10^{13}[s^{-1}]$ is the interstitial frequency jump, R is the ideal gas constant, E_{im} is the interstitial migration energy ranging between 0.5 and 2.0 [eV] and T is the absolute temperature [8,29,30]. The vacancy bulk diffusion coefficient (D_v) can be obtained using the self-diffusion coefficient (D_U). The self-diffusion process may be expressed as a superposition of the vacancies and interstitials migration mechanisms so that:

$$D_U \approx D_vC_v + D_iC_i \tag{34}$$

Studies carried out by Matzke [31] concluded that below 1273 K the self-diffusion mechanism is athermal and it depends linearly on the fission rate at which the sample is irradiated. As the temperature increases above 1273 K, the coefficient approaches its purely thermal value. For that reason, it can be represented as the superposition of both effects:

$$D_U = A\dot{F} + D_{U0}\exp\left(-\frac{E_U}{RT}\right) \tag{35}$$

where $A = 1.2 \times 10^{-39}m^5$ is a semi-empirical constant estimated by Matzke [31,32], D_{U0} is the pre-exponential constant and E_U is the self-diffusion migration energy. Table 1 shows values for the thermal parameters of the self-diffusion coefficient reported by Veshchunov et al. [8], by Matzke [33] and by Marin et al. [34]. The latter authors report experimental data of the self-diffusion coefficients of UO_{2+x} in terms of x, which is here extrapolated to $x = 0$.

Grain boundary diffusion is involved in the densification process of intergranular pores and its coefficient is modeled using an

Table 1
Parameters for thermal self-diffusion coefficient in UO_2.

D_{U_0} (m^2/s)	E_U/R (K)	Reference
2×10^{-4}	64200	[8]
6.5×10^{-5}	65000	[33]
5.4×10^{-9}	42800	[34]

Table 2
Parameters for grain boundary self-diffusion coefficient in UO_2.

Temperature (K)	D_{UGB0} (m^2/s)	E_{UGB}/R (K)	Recalculated from
1523–1973	1.5×10^{-6}	28900	[35]
1750–1923	6.14×10^{-6}	35400	[36]
2173–2423	$3.18 \times 10^{-15}/w$	22900	[37]

Arrhenius expression:

$$D_{UGB} = D_{UGB0} \exp\left(-\frac{E_{UGB}}{RT}\right) \tag{36}$$

Different values based on data reported in the literature for the pre-exponential factor (D_{GB0}) and the grain boundary migration energy (E_{UGB}) are listed in Table 2, where w is the grain boundary width.

According to Fisher [38], the quotient between the diffusion coefficients in grain boundary and bulk, D_{GB}/D, is about 10^5 and 10^6. On this basis, it is also reasonable to adopt the approximation $D_{UGB} \approx D_U \times 10^5$.

The parameters of the self-diffusion coefficients D_U and D_{UGB} were fitted with a subset of the densification data of isothermal experiments carried out between 1473 K and 1973 K [39] for which the initial pore distribution had been reported. The best agreement is obtained with:

$$D_U\left[m^2/s\right] = \begin{cases} 2 \times 10^{-4} \exp\left(\frac{64200}{T}\right) & T < 1500\ K \\ 5.4 \times 10^{-9} \exp\left(\frac{42800}{T}\right) & T \geq 1500\ K \end{cases} \tag{37}$$

$$D_{UGB}\left[m^2/s\right] = \begin{cases} 20 \exp\left(\frac{64200}{T}\right) & T < 1800\ K \\ 6.14 \times 10^{-6} \exp\left(\frac{35400}{T}\right) & T \geq 1800\ K \end{cases} \tag{38}$$

Based on the work developed by Griesmeyer and Ghoniem [27], vacancies and interstitials (dimensionless) concentrations in thermodynamic equilibrium can be estimated using the Arrhenius expressions:

$$C_v^{eq} = 2 \times \exp(-3.3(\mathrm{eV})/k_bT) \tag{39}$$

$$C_v^{eq} = 0.5 \times \exp(-6.2(\mathrm{eV})/k_bT) \tag{40}$$

At a pore surface the interstitials concentration is assumed zero while that of vacancies might be calculated as [1,6]:

$$C_v^{ps} = C_v^{eq} \exp(-\Omega\Delta P/k_bT) \tag{41}$$

where ΔP is the pressure difference at the pore surface, given by:

$$\Delta P^a = p_{in}^a - p_h - 2\gamma/r_p^a \tag{42}$$

$$\Delta P^e = p_{in}^e - p_h - 2\gamma f_S/\left(r_p^e f_V\right) \tag{43}$$

where $p_{in}^{a,e}$ is the inner gas pressure that can be evaluated using the van der Waals equation $p_{in}(V_p - n_g^0 b_{vw}) = n_g^0 RT$, p_h is the hydrostatic pressure and $\gamma = 0.3485 - 5.74 \times 10^{-5}(T - 273)$ is the pore surface tension [8,21].

The pore size evolution is controlled by the net flux of point defects. Vacancies arriving at the cavity will contribute to its growth and vacancies leaving and interstitials getting into the pore will result in its shrinkage. In addition to the bulk processes for intergranular pores, the grain boundary diffusion must be incorporated into the model. Then, the rate of change of the pore radius is:

$$\frac{dr_p^a}{dt} = \frac{1}{r_p^a} D_v(C_v - C_v^{ps}) - \frac{1}{r_p^a} D_i C_i - \frac{\left(r_p^a + r_{int}\right)^2}{2r_p^{a2}} \Omega \dot{F} \eta \lambda f_{sat} f_{vl} \tag{44}$$

$$\frac{dr_p^e}{dt} = \frac{1}{r_p^e f_V}\left[D_v(C_v - C_v^{ps}) - D_i C_i + wD_{UGB}\frac{\Omega\Delta P^e}{k_b T r_p^e} - \frac{\left(r_p^e + r_{int}\right)^2}{2r_p^e} \Omega \dot{F} \eta \lambda f_{sat} f_{vl}\right] \tag{45}$$

where the grain boundary width w is chosen as twice the lattice parameter.

2.2.2. Densification due to thermal effects

Starting from the model exposed in section 2.2.1, a simplified formulation to evaluate porosity evolution under isothermal conditions without irradiation is presented below. In these conditions point defects concentrations tend towards thermodynamic equilibrium values. From Eq. (34), we have:

$$1 \approx \frac{D_v C_v^{eq}}{D_U} + \frac{D_i C_i^{eq}}{D_U} \tag{46}$$

For temperatures below 2000 K the relation $D_i C_i^{eq}/D_U$ takes values less than 10^{-6} and the interstitial effect can be neglected. So then:

$$D_U \approx D_v C_v \tag{47}$$

If in equations (31), (44) and (45) the contributions of interstitials and irradiation are neglected, we find:

$$\frac{\partial C_v}{\partial t} = \sum_{k=1}^{n}(S_{pv_k} D_v C_v^{ps}) + \sum_{l=1}^{m}(S_{pv_l} D_v C_v^{ps}) + (S_{dv} + S_{BGv}) D_v C_v^{eq} - S_{tv} D_v C_v \tag{48}$$

$$\frac{dr_p^a}{dt} = \frac{1}{r_p^a} D_v(C_v - C_v^{ps}) \tag{49}$$

$$\frac{dr_p^e}{dt} = \frac{1}{r_p^e f_V}\left[D_v(C_v - C_v^{ps}) + wD_{UGB}\frac{\Omega\Delta P^e}{k_b T r_p^e}\right] \tag{50}$$

2.2.3. Densification indicators

Quantification of densification is usually made by using the relative volume change ($\Delta V/V_0$), the relative density change ($\Delta\delta/\delta_0$) or simply the density change ($\Delta\delta$) as indicators [3,17].

Considering that $\delta = m/V$, the relative density change is:

$$\frac{\Delta\delta}{\delta_0} = \frac{\delta_f - \delta_0}{\delta_0} = \frac{m_f / V_f - m_0/V_0}{m_0/V_0} \tag{51}$$

where the subscripts 'o' and '*f*' stand for the initial and final states, respectively; $m_{0,f}$ and $V_{0,f}$ are the mass and volume of the material. Assuming that the mass remains unchanged during the process, then:

$$\frac{\Delta\delta}{\delta_0} = \frac{V_0}{V_f} - 1 \tag{52}$$

The relative volume change can be expressed as:

$$\frac{\Delta V}{V_0} = \frac{V_f - V_0}{V_0} = \frac{V_f}{V_0} - 1 \tag{53}$$

Combining equations (52) and (53), then:

$$\frac{\Delta\delta}{\delta_0} = \frac{-\Delta V/V_0}{1 + \Delta V/V_0} \tag{54}$$

Taking into account the contributions of all pore classes, the initial and final material volumes are given by:

$$V_0 = V_s + \sum_{k=1}^{n} V_{0_k}^a + \sum_{l=1}^{m} V_{0_l}^e \tag{55}$$

$$V_f = V_s + \sum_{k=1}^{n} V_{f_k}^a + \sum_{l=1}^{m} V_{f_l}^e \tag{56}$$

where V_s is the volume occupied by the solid material and $V_{(0,f)_j}^{(a,e)}$ is the volume contributed by pore class j with $j = k$ or l. Using equations (53), (55) and (56), an expression for the relative volume change as a function of the radii of the pore classes and the respective initial porosities is obtained

$$\frac{\Delta V}{V_0} = -\sum_{k=1}^{n} P_{0_k}^a \left[1 - \left(\frac{r_{f_k}^a}{r_{0_k}^a}\right)^3\right] - \sum_{l=1}^{m} P_{0_l}^e \left[1 - \left(\frac{r_{f_l}^e}{r_{0_l}^e}\right)^3\right] \tag{57}$$

where the porosity for pore class j is:

$$P_{0_j}^{(a,e)} = \frac{V_{0_j}^{(a,e)}}{V_s + \sum_{k=1}^{n} V_{0_k}^a + \sum_{l=1}^{m} V_{0_l}^e} \tag{58}$$

Table 3 summarizes the different parameters and variables used in the model.

2.2.4. Parametric analysis of the model

The response of the model to variations in its significant parameters has been tested before applying it to the simulation of experimental cases. Firstly, the thermal model has been analyzed by running the code for different values of the more influencing parameters: temperature, grain radius and initial pore size distribution. The former clearly affects the diffusion of vacancies and interstitials to and from the pores, which are thermally activated processes. The two latter are crucial parameters to describe the densification kinetics.

Certain assumptions have to be made on the pore distribution to carry out the simulation. A total initial porosity of 5% is postulated, which falls within the fabrication margins. Besides that, average grain sizes of 5 and 10 μm are proposed. For simplicity, monomodal distributions are assumed and two types are analyzed: one purely intragranular and another purely intergranular. In addition, the median volume pore radius is, within the model, the characteristic parameter of the distribution; the values 0.25 and 0.50 μm are assumed for it.

Fig. 1 presents the relative volume change due to densification as a function of time for different distributions and temperatures. The simulations were performed assuming 200 h long treatments under isothermal conditions. In general, densification is faster at higher temperatures. In Fig. 1 a) the densification achieved in materials containing only intragranular pores is shown. Examples with different initial distributions are given. It can be seen that materials with smaller grain radius densify faster. For instance, the densification achieved after 200 h at 1973 K is approximately −0.8% for a material with average grain radius of 5 μm, while it is about −0.65% if the grain radius is of 10 μm in the average. Similarly, Fig. 1 b) shows the comparison of a material containing only intergranular pores. Generally speaking, these pores have a more noticeable effect on densification than the intragranular pores and, for the highest temperature tested and the lowest median pore radius, the fabrication pores completely vanish after a thermal treatment of about 20 h. If only intergranular pores are present, the model predicts that a modification in the grain size has a negligible effect on densification (superimposed curves). It is also observed in Fig. 1a) and b) that a shift towards higher values in the initial pore size distribution (increase in r_{med}) delays the densification, either for intra or intergranular pores. The difference in behavior between both types of pores with respect to the magnitude of densification may be attributed to the fact that for intergranular pores the grain boundary diffusion mechanism operates.

The parametric analysis of the model with irradiation includes other aspects besides those of the thermal model. The simulations were performed up to burnups of about 0.55 MW d/kgU, assuming isothermal conditions and the values listed in Table 4 for the given parameters.

The study carried out in the present work includes also the number of defects that can escape from a damage cascade (Y_{vi}) and the number of vacancies released from a pore after its interaction with a fission fragment (η). Different authors report for them values in a wide range on the basis of experimental results or estimations: Y_{vi} between 10^4 and 5×10^5 [19,20] and η with an upper limit of 600 [4]. The present examination intends to establish for them narrower ranges of interest. These parameters were fitted with the densification data of irradiated samples that had reached a maximum centerline temperature of 1600 K and whose initial pore distribution had been informed [39]. The best fitting with the experimental results is obtained with $Y_{vi} = 5 \times 10^5$ and $\eta = 400$ as can be appreciated in section 3.

3. Results and discussion

Densification measurements carried out in UO_2 pellets with different microstructures are presented by Freshley et al. [3,37]. Differences in the microstructures are given by the initial percentage of porosity, average grain size, average pore size and type of distribution. In the present paper, the nomenclature used by Freshley to identify the samples is adopted, designating each different microstructure as a "fuel type". As stated before, in order to make comparisons between experimental data and model predictions, it is necessary to have a good representation of the pore

Table 3
List of parameters and variables used in the model.

Symbol	Description	Units	Used value
A	Semi-empirical constant for radiation enhance self-diffusion	m^5	$1{,}2 \times 10^{-39}$ [30,31]
a	UO_2 lattice parameter	m	$5{,}47 \times 10^{-10}$ [1]
b	Burgers vector	m	$\sqrt{2}a/2$ [40]
b_{vw}	van der Waals volumetric constant (For H_2)	m^3/mol	$2{,}65 \times 10^{-5}$ [41]
C_i	Interstitials fractional concentration in the bulk	–	–
C_i^{eq}	Interstitials fractional concentration in thermodynamic equilibrium	–	–
C_v	Vacancies fractional concentration in the bulk	–	–
C_v^{eq}	Vacancies fractional concentration in thermodynamic equilibrium	–	–
C_v^{ps}	Vacancies fractional concentration at the pore surface	–	–
C_{vsat}	Saturation vacancies concentration	mol/m^3	10 [21]
D_i	Interstitial diffusion coefficient of uranium in UO_2	m^2/s	–
D_U	Self-diffusion coefficient of uranium in UO_2	m^2/s	–
D_{U0}	Pre-exponential constant for the self-diffusion coefficient of uranium in UO_2	m^2/s	–
D_{UGB}	Grain boundary self-diffusion coefficient of uranium in UO_2	m^2/s	–
D_{UGB0}	Pre-exponential constant for grain boundary self-diffusion coefficient of uranium in UO_2	m^2/s	–
D_v	Vacancy diffusion coefficient of uranium in UO_2	m^2/s	–
E	Elastic Modulus of UO_2	Pa	–
E_{im}	Interstitial migration energy of uranium in UO_2	eV	0.5 [30]
E_U	Self-diffusion migration energy of uranium in UO_2	eV	–
E_{UGB}	Grain boundary self-diffusion migration energy of uranium in UO_2	eV	–
$\dot{F}$	Fission rate	$Fis/m^3.s$	–
f_A	Pore area shape factor	–	–
f_V	Pore area volume factor	–	–
f_{vl}	Vacancies volume fraction within a pore	–	–
f_{sat}	Vacancies saturation function	–	–
G	Shear modulus of UO_2	Pa	–
k_b	Constante de Boltzmann	J/K	$1{,}38 \times 10^{-23}$
m	Fuel mass	kg	–
N_p	Pore concentration for a given pore class	m^{-3}	–
n_g^0	Initial number of gas moles within a pore	mol	–
p_h	Hydrostatic pressure	Pa	10^5 [3]
$P_{in}^{(a,e)}$	Inner sintering gas pressure	Pa	–
P_T	Fractional fuel total porosity	–	–
R	Ideal gas constant	J/mol.K	8.314
R_c	Minimum radius detected experimentally	m	2.5×10^{-8} [3]
R_g	Grain radius	m	–
R_t	Minimum radius accounted in the code	m	5×10^{-9}
r_a	Dislocation core radius	m	–
$r_{cd(i)}$	Radius of the spontaneous capture of interstitials by dislocations	m	-
$r_{cd(v)}$	Radius of the spontaneous capture of vacancies by dislocations	m	-
r_{int}	Range of interaction of a pore with a fission fragment	m	1×10^{-9} [22]
r_{medv}	Median volume pore radius	m	–
r_{md}	Mean half distance between dislocations	m	–
r_{mv}	Mean volume pore radius	m	–
r_p^a	Intragranular pore radius	m	–
r_p^e	Intergranular pore radius	m	–
r_{vi}	Vacancy-interstitial recombination distance	m	a
$S_{d(i)}$	Dislocation sink strength for interstitials	m^{-2}	–
$S_{d(v)}$	Dislocation sink strength for vacancies	m^{-2}	–
$S_{GB(i)}$	Grain boundary sink strength for interstitials	m^{-2}	–
$S_{GB(v)}$	Grain boundary sink strength for vacancies	m^{-2}	–
$S_p^{(a,e)}{}_j$	Intra (inter)-granular pore sink strength	m^{-2}	–
$S_{t(i)}$	Total sink strength for interstitials	m^{-2}	–
$S_{t(v)}$	Total sink strength for vacancies	m^{-2}	–
T	Temperature	K	–
V	Total fuel volume	m^3	–
V_p	Pore volume for a given pore	m^3	–
V_s	Volume occupied by the solid fuel material	m^3	–
w	Grain boundary width	m	$2a$
Y_{vi}	Point defects number escaping a damage cascade	–	$5 \times 10^{5*}$
z_i	Dislocation bias factor for interstitials	–	–
z_v	Dislocation bias factor for vacancies	–	1.00 [22]
α	Vacancy-interstitial recombination constant	m^{-2}	–
γ	Surface tension	J/m	–
ΔV_i	Realaxation volume caused by a uranium insterstitial	m^3	6.0×10^{-30} [24]
ΔV_v	Relaxation volume caused by a uranium vacancy	m^3	-2.2×10^{-30} [24]
δ	Fuel density	kg/m^3	–
η	Number of vacancies that a pore can emit in a single pore-spike interaction	–	400*
θ	Dihedral angle	°	50 [14]
λ	Fission fragment track length	m	1×10^{-6} [8]
μ	Poisson ratio of UO_2	–	–
ν_i	Interstitial jump frequency	s^{-1}	10^{13} [8]

(*continued on next page*)

Table 3 (*continued*)

Symbol	Description	Units	Used value
ρ	Projection radius	m	–
ρ_D	Dislocations density	m^{-2}	–
Ω	UO_2 atomic volume	m^3	4.09×10^{-29} [1]

* Fitted to data in the present work.

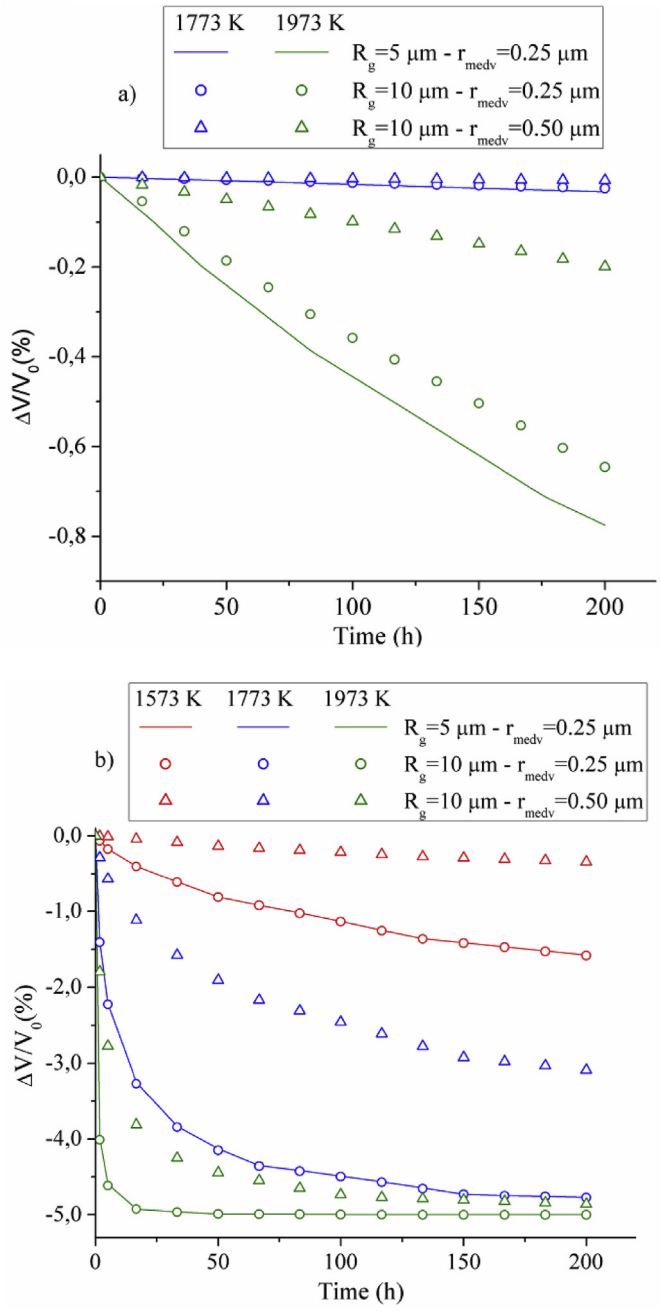

Fig. 1. Relative volume change at different temperatures using the thermal model. a) an intragranular pore distribution and b) an intergranular pore distribution.

distributions for each type of fuel. Some examples of the fitting obtained in the present work of the pore distributions, using the equations displayed in section 2.1 are presented here.

The parameters D_U, D_{UGB}, Y_{vi} and η were fitted on the basis of the densification results reported for fuel type 4 [3], for which the pore distribution is well characterized. Then, the same set of parameters was used to simulate the other experiments carried out on samples with microstructures different to that of fuel type 4.

Table 4
Values adopted for the more significant parameters used in the present analysis.

Parameter	Value
R_g	5×10^{-6} m
r_{medv}	5×10^{-7}m
$\dot{F}$	10^{19} fis/m^{3}s
λ	10^{-6} m
p_h	10^5 Pa
T	773 to 1973 K

Fig. 2 shows a comparison between the simulated distributions and the experimental values reported by Brite et al. in the EEI/EPRI Fuel Densification Project [39] for fuel types 1, 4 and 6. Fig. 2 a) shows the porosity as a function of the pore classes while in Fig. 2 b) the accumulated porosity is presented. In both cases, the full lines are the spline interpolations of the calculated results. It is important to notice that the porosity values corresponding to each pore class will be affected by the law used to discretize the radius, which in this case is carried out with equation (11). The effect of the discretization law is less noticeable in the accumulated porosity plot. In that sense, even though in Fig. 2 a) the simulations present a perceptible departure from some experimental points, a good agreement is observed in Fig. 2 b) in the whole range.

3.1. Results for isothermal tests without radiation

Generally speaking, the model presented in section 2.2.2 predicts that the smaller pores tend to disappear during the re-sintering process, and consequently the mean value of the pore distribution shifts towards greater radius.

This model was employed to simulate re-sintering experiments performed in the EEI/EPRI Fuel Densification Project [39] involving pellets with different microstructures. They were heated at a rate of 200 K/h up to final temperatures between 1473 and 1973K at which they were held during 4–1500 h. The final pellet density was measured by water immersion. No correction was introduced to account for the heating and cooling times. From these data, those that had an appreciable density change were selected to make comparisons with the model results. The simulations were carried out assuming a material with grains uniform in size and equal to its average. The finite differences method was used to solve the differential equations displayed in section 2.2.2.

Fig. 3 shows the comparison between experimental data and predictions of the density change as a percentage of the theoretical density achieved in isothermal treatments for temperatures between 1773 and 1973 K after 4, 14 and 48 h. In general terms, the results obtained are in good agreement with experiments and about 92% of the cases studied presented an absolute departure of less than 1%TD from the line of perfect agreement.

In Fig. 4 the density change of pellets with different microstructure is represented as a function of the duration of the

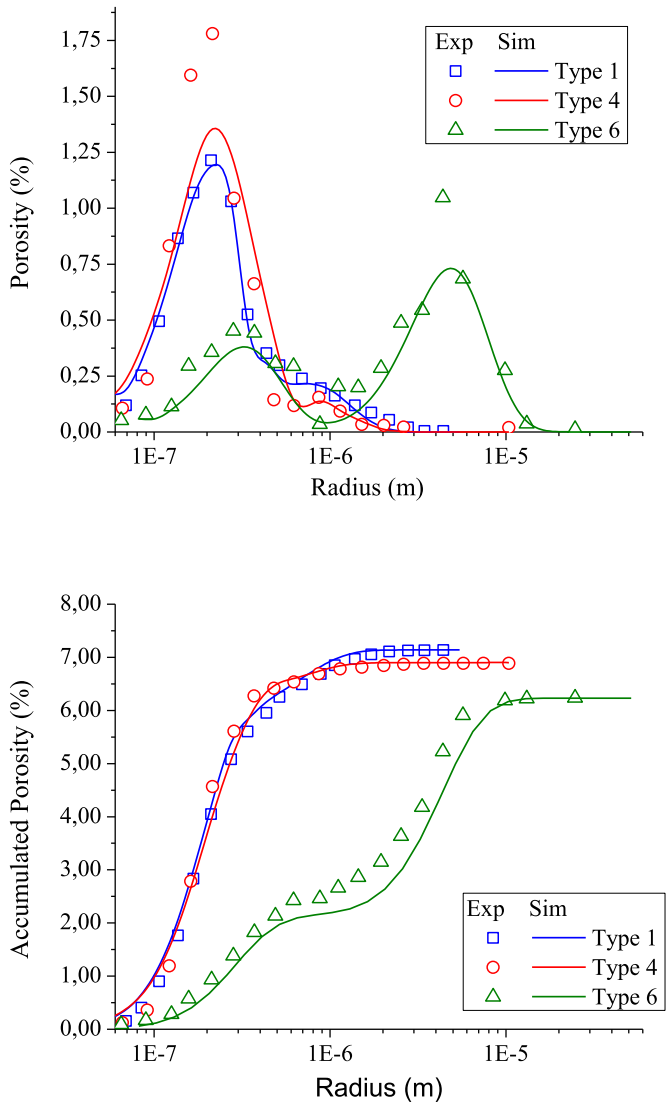

Fig. 2. Comparison between experimental data [3,37] and simulation of pore distributions for different fuel microstructures as functions of the pore radius; a) porosity, b) accumulated porosity.

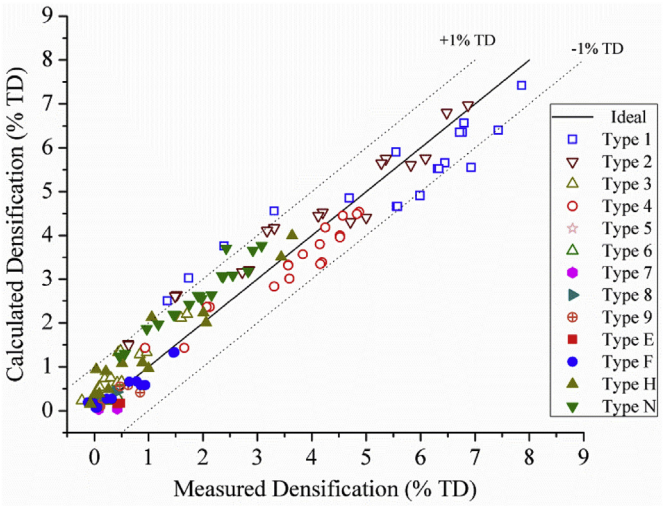

Fig. 3. Comparison between calculated and measured densification achieved in isothermal treatments of samples with different microstructures [39].

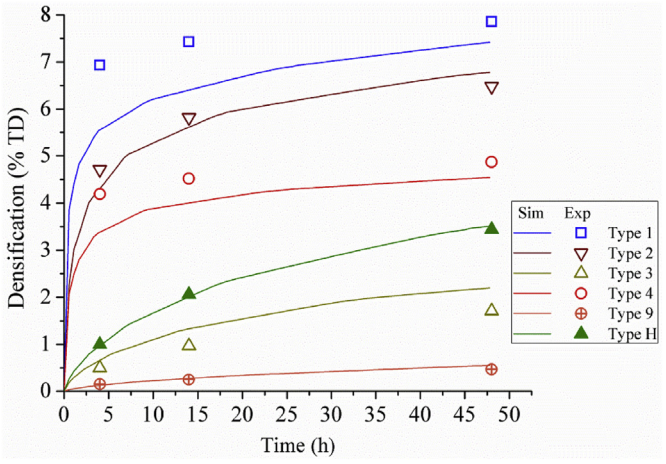

Fig. 4. Densification vs. time of isothermal treatments at 1973 K of samples with different microstructures [39].

isothermal treatments. The experiments consisted of heating the samples at a rate of 200 K per hour up to the test temperature of 1973 K. In general, the simulated results agree quite well with the experimental data. Nevertheless, a certain underprediction of the densification can be observed, particularly for the fuels labeled as Types 1 and 4 with relative deviations up to 20%. This can be attributed to the fact that these fuels have the highest proportion of small pores and the lowest grain sizes, in which cases some degree of densification most probably occur during the heating ramps, that is not accounted for in the simulations.

3.2. Results for irradiation tests

The model introduced in section 2.2.1 was used to simulate experiments under irradiation performed in the EEI/EPRI Fuel Densification Project [39]. The linear irradiation power was controlled in order that the centerline temperature did not exceed about 1673 K during the whole tests. The final pellet density was measured in a hot-cell by means of a mercury pycnometer.

Fig. 5 shows the comparison between experimental data and predictions of the density changes (%TD) of fuel pellets irradiated during 446 and 1600 h reaching center temperatures between 573 and 1598 K. Although there are some deviations, the results obtained are generally in good agreement with experiments and about 67% of the simulated cases presented an absolute departure of less than 1%TD from the line of perfect agreement. It must be noticed that a fuel pellet under irradiation develops a temperature gradient which influences the densification rate at the different sample radii. For simplicity, the model assumes a material with uniform grains of size equal to its average. In addition, the centerline pellet temperature is assumed to hold in the whole pellet. These simplifications can give rise to the differences observed in Fig. 5.

Fig. 6 presents a comparison between simulations of some of the experimental data reported by Brite et al. [39] performed with the model in this work and by Dollins [5]. It shows that with the present model about 75% of the compared values have departures of the ideal case of less than 1% TD while for Dollins only 38% fall within this range. The main difference between both models is that Dollins evaluates the densification for a single pore class while in this work a pore size distribution is used.

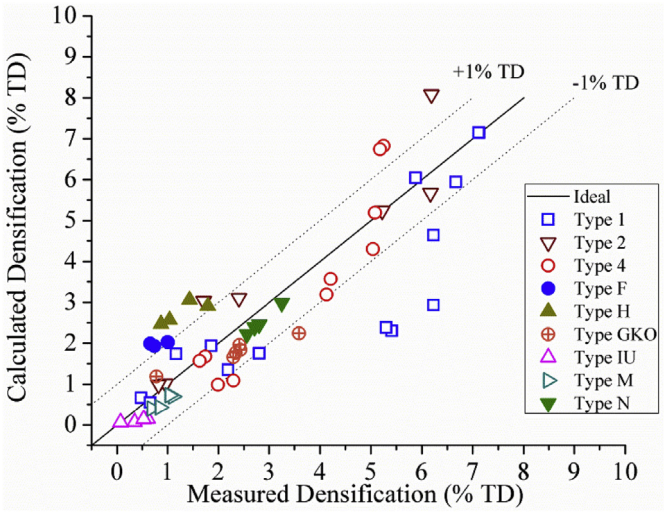

Fig. 5. Comparison between calculated and measured densification achieved in irradiated samples with different microstructure [39].

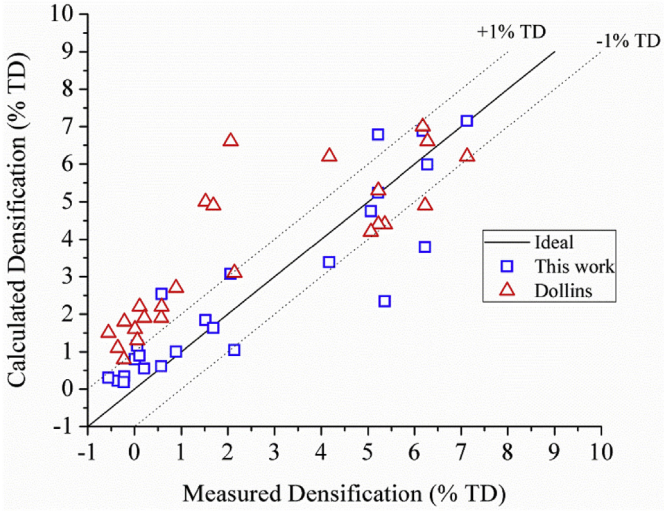

Fig. 6. Comparison between calculated and measured densification achieved in irradiated samples with different microstructures, using the model by Dollins [5] and the model presented in section 2.2.1.

4. Conclusions

A model to evaluate the fuel pellets densification under irradiation conditions is presented in this work. The model takes into account the point defects diffusion processes and the interaction between the fission fragments and the as-fabricated pores. In addition, using suitable simplifications a model to determine fuel pellets densification under isothermal conditions is obtained.

For the thermal model, the influence of pores size distribution and temperature were analyzed. This study has shown that an intergranular distribution causes greater densification values than an intragranular one with the same parameters; this may be associated to the grain boundary diffusion phenomenon that is active for pores located at the grain perimeter. If the pore size distribution is shifted towards higher values, the pore shrinkage achieved is lower. Furthermore, for all cases studied it was observed that the densification increases with temperature.

The model was also compared with data collected in experiments under irradiation. It was concluded that the fitting is optimized when $Y_{vi} = 5 \times 10^5$ and $\eta = 400$ are chosen.

Both the thermal and the irradiation model were tested using experimental data provided by the EPRI Project. In all cases, the simulations were carried out by solving the equations involved considering grains of average size and isothermal conditions. A good agreement was obtained between the calculated and measured results. In addition, the model presented in this paper was compared with a model presented by Dollins, concluding that the former provides a better fit for the cases evaluated. The explanation can be found in the inclusion in our model of a pore size distribution function, which provides a better representation of the physical reality, instead of the single pore type considered by that author.

The next step of this work will be to incorporate the densification model as a subroutine of the DIONISIO code, which already contains a model for bubble formation by fission gases and release of these to the free volume of the fuel rod. This will allow testing the combined effects of densification and swelling. Moreover, given the strong temperature gradient that develops in the fuel pellets, a local calculation of densification is necessary to obtain realistic predictions. This will be possible within the frame of the general code which will provide adequate local values of all the significant physical parameters.

References

[1] D.R. Olander, Fundamental Aspects of Nuclear Reactor Fuel Elements, 1976.
[2] H. Assmann, H. Stehle, Thermal and in-reactor densification of UO_2: mechanisms and experimental results, Nucl. Eng. Des. 48 (1) (1978) 49–67.
[3] M.D. Freshley, D.W. Brite, J.L. Daniel, P.E. Hart, Irradiation-induced densification of UO_2 pellet fuel, J. Nucl. Mater. 62 (2–3) (1976) 138–166.
[4] C.C. Dollins, F.A. Nichols, In-pile intragranular densification of oxide fuels, J. Nucl. Mater. 78 (2) (1978) 326–335.
[5] C.C. Dollins, In-pile densification of intergranular porosity in oxide fuels, J. Nucl. Mater. 82 (1993) 494–500.
[6] Y. Bouguerra, A. Si-Ahmed, A model for predicting evolution of pore size distributions in UO2 fuel, J. Nucl. Mater. 178 (2–3) (1991) 300–305.
[7] Lindman, On the rate of in-reactor UO_2 densification, J. Nucl. Mater. 71 (1977) 73–77.
[8] M.S. Veshchunov, V.E. Shestak, Model for evolution of crystal defects in UO_2 under irradiation up to high burn-ups, J. Nucl. Mater. 384 (1) (2009) 12–18.
[9] V.I. Tarasov, M.S. Veshchunov, Models for fuel porosity evolution in UO_2 under various regimes of reactor operation, Nucl. Eng. Des. 272 (2014) 65–83.
[10] X. Iltis, M. Ben Saada, H. Mansour, N. Gey, A. Hazotte, N. Maloufi, A new characterization approach for studying relationships between microstructure and creep damage mechanisms of uranium dioxide, J. Nucl. Mater. 474 (2016) 1–7.
[11] H. Matzke, T. Inoue, R. Warren, The surface energy of UO_2 as determined by hertzian indentation, J. Nucl. Mater. 91 (1) (1980) 205–220.
[12] A.M. Ross, Irradiation behaviour of fission-gas bubbles and sintering pores in UO_2, J. Nucl. Mater. 30 (1969) 134–142.
[13] V.I. Tarasov, M.S. Veshchunov, Modelling of as-fabricated porosity in UO_2 fuel by MFPR code, Eur. Phys. J. Nucl. Sci. Technol. 2 (2016) 19.
[14] R.J. White, M.O. Tucker, A new fission-gas release model, J. Nucl. Mater. 118 (1) (1983) 1–38.
[15] K. Leschonski, Representation and evaluation of particle size analysis data, Part. Char. 1 (3) (1984) 89–95.
[16] V.D. Ozrin, V.I. Tarasov, Model for evolution of as-fabricated pores in UO_2 fuel under irradiation conditions, in: L.A. Bolshova (Ed.), In Models For Fission Products Release From Irradited UO_2 Fuel, 2008.
[17] H. Stehle, H. Assmann, The Dependence of in-reactor UO_2 densification on temperature and microstructure, J. Nucl. Mater. 52 (1974) 303–308.
[18] H. Stehle, H. Assmann, In-Reactor UO_2 densification, J. Nucl. Mater. 61 (1976) 326–329.
[19] A. Denis, R. Piotrkowski, Simulation of isothermal gas release, J. Nucl. Mater. 229 (1996) 149–154.
[20] T. Nakajima, H. Saito, A comparison between fission gas release data and FEMAXI-IV code calculations, Nucl. Eng. Des. 101 (3) (1987) 267–279.
[21] A. Bouloré, Étude et modelisation de la densification en pile des oxydes UO_2 et MOX, Institut National Polytechnique de Grenoble, 2001.
[22] G. Khvostov, K. Mikityuk, M.A. Zimmermann, A model for fission gas release and gaseous swelling of the uranium dioxide fuel coupled with the FALCON code, Nucl. Eng. Des. 241 (8) (2011) 2983–3007.
[23] A.D. Brailsford, R. Bullough, The theory of sink strengths, Phil. Trans. Roy. Soc. Lond. 302 (1981).
[24] V.G. Baranov, A.V. Lunev, A.V. Tenishev, A.V. Khlunov, Interaction of dislocations in UO_2 during high burn-up structure formation, J. Nucl. Mater. 444

(1–3) (2014) 129–137.
[25] A. Soba, A. Denis, Simulation with DIONISIO 1.0 of thermal and mechanical pellet-cladding interaction in nuclear fuel rods, J. Nucl. Mater. 374 (1–2) (2008) 32–43.
[26] W.G. Wolfer, On the coefficient for bulk recombination of vacancies and interstitials, Computer (Long. Beach. Calif). 99 (1981) 117–123.
[27] J.M. Griesmeyer, N.M. Ghoniem, The response of fission gas bubbles to the dynamic behavior of point defects, J. Nucl. Mater. 80 (1979) 88–101.
[28] J.M. Griesmeyer, N.M. Ghoniem, A dynamic intragranular fission gas behavior model, J. Nucl. Mater. 55 (1979) 69–95.
[29] A.S. Boyarchenkov, S.I. Potashnikov, K.A. Nekrasov, A.Y. Kupryazhkin, Investigation of cation self-diffusion mechanisms in $UO_{2\pm x}$ using molecular dynamics, J. Nucl. Mater. 442 (1–3) (2013) 148–161.
[30] J.R. Matthews, Technological problems and the future of research on the basic properties of actinide oxides, J. Chem. Soc. Faraday. Trans. 2 83 (7) (1987) 1273.
[31] H. Matzke, Radiation enhanced diffusion in UO_2 and (U, Pu)O_2, Radiat. Eff. 75 (1–4) (1983) 317–325.
[32] H. Matzke, Atomic transport properties in UO_2 and mixed oxides (U, Pu)O_2, J. Chem. Soc. Faraday. Trans. 2 83 (7) (1987) 1121.
[33] H. Matzke, Atomic mechanisms of mass transport in ceramic nuclear fuel materials, J. Chem. Soc. Faraday. Trans. 86 (8) (1990) 1243–1256.
[34] J.F. Marin, P. Contamin, Uranium and oxygen self-diffusion in UO_2, J. Nucl. Mater. 30 (1–2) (1969) 16–25.
[35] G.L. Reynolds, B. Burton, Grain-boundary diffusion in uranium dioxide: the correlation between sintering and creep and a reinterpretation of creep mechanism, J. Nucl. Mater. 82 (1) (1979) 22–25.
[36] IAEA, Thermodynamics vol. II, in: In Thermodynamics, 1966.
[37] S. Yajima, H. Furuya, T. Hirai, Lattice and grain-boundary diffusion of uranium in UO_2, J. Nucl. Mater. 20 (2) (1966) 162–170.
[38] J.C. Fisher, Calculation of diffusion penetration curves for surface and grain boundary diffusion, J. Appl. Phys. 22 (1) (1951) 74–77.
[39] D.W. Brite, J.L. Daniel, N.C. Davis, M.D. Freshley, P.E. Hart, R.K. Marshall, EEI/EPRI Fuel Densification Project, 1975.
[40] J. Rest, Derivation of analytical expressions for the network dislocation density, change in lattice parameter, and for the recrystallized grain size in nuclear fuels, J. Nucl. Mater. 349 (1–2) (2006) 150–159.
[41] D.R. Lide, CRC Handbook of Chemistry and Physics, EBook, 2003, p. 3485.